SOME PROBLEMS CONNECTED WITH THE USE OF INTERSECTING PROTON STORAGE RINGS

K. Johnsen, W. C. Middelkoop, B. de Raad, L. Resegotti, A. Schoch, K. R. Symon, C. J. Zilverschoon*

CERN

(Presented by B. de RAAD)

1. INTRODUCTION

Soon after the successful operation of the CERN PS it was realised, that its good beam quality and high intensity would make it attractive to consider the feasibility of colliding beam experiments. A first design study for a set of intersecting proton storage rings (ISR) for the CERN PS has been presented at the previous Accelarator Conference [1]. Since then our design study for the ISR has been continued and its main emphasis has been placed on their utilisation.

The experimental problems connected with the utilisation of ISR are quite different from those which are familiar from stationary target experiments with existing accelerator. Collisions between protons take place inside the ISR vacuum chamber and must be studied by analyzing their reaction products in detectors placed around the vacuum chamber near the interaction region. This restricts the freedom in the choice of the experimental conditions. In this paper we shall discuss in some detail a few specific experiments in order to show that intersecting beam experiments are feasible. This will also give the occasion to point out some features that should be incorporated in an ISR design in order to increase its flexibility for experiments.

* On leave of absence from MURA, Madison, Wisconsin, U. S. A. Ford Foundation Fellow.

2. INTERSECTING STORAGE RINGS FOR THE CERN PS

The layout of a pair of ISR for the CERN PS is shown in Fig. 1. The ISR are concentric with 8 interaction regions. Originally [1] a pair of excentris ISR, with only two interaction regions had been considered, but a more

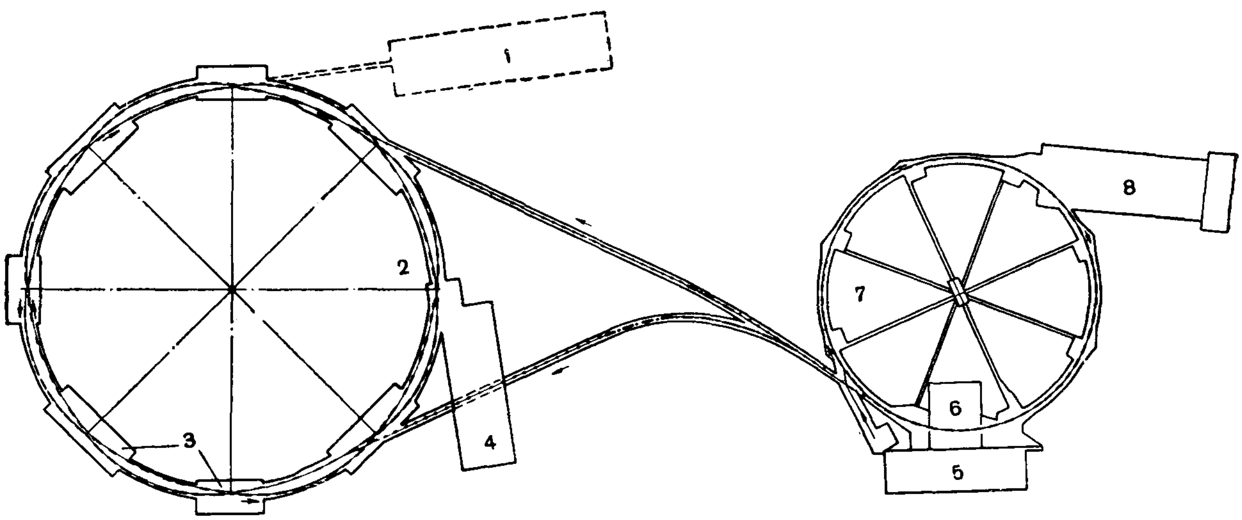

Fig. 1. CERN proton synchrotron with concentric storage rings:
1 — external target hall; *2* — concentric storage rings; *3* —colliding beam areas; *4* — internal target hall; *5* — south hall; *6*— north hall; *7* — proton synchrotron; *8* — east hall.

detailed study has shown that the concentric design proposed by O'Neill [2] is entirely feasible and is therefore preferable on account of the larger number of experiments which can be carried out simultaneously. This is important because some experiments may have low counting rates and require long running times. An experimental setup may often require important modifications to the ISR vacuum system or magnet units and this makes it difficult to change rapidly from one experiment to another. It is also possible to choose a different layout of the accelerator components and buildings around different interaction regions so that each can be adopted to specific experiments.

The position of the ISR with respect to the CERN PS is determined by the available site. As shown in Fig. 1 the ring tunnel has been widened around the interaction regions to make room for experimental equipment. We shall come back to this point later. Since each storage ring can be used as a beam stretcher for the CERN PS, Fig. 1 also shows two stationary target halls, but these are not relevant for the present discussion. The total energy of the protons in the ISR is variable from 10 GeV to 28 GeV. The figures given in this report are valid for a total energy of 25 GeV. At this energy the beam characteristics in the interaction region are

Beam width	variable from 1.5 to 6 cm
Beam height	1 cm
Total momentum spread	2.5%
Circulating beam current	20 A
Interaction rate ($\sigma=40$ mb)	1.6×10^{5} events/s

The normal stack width is 6 cm, but by applying a suitable gradient perturbation [3] the closed orbits for different momenta can be superposed in the interaction region with a corresponding increase of the stack width elsewhere so that a beam width of about 1.5 cm results. This Terwilliger scheme can be used in two ways. The simplest is to inject under normal conditions until a current of 20 A has been reached. Subsequently the quadrupoles for its scheme are excited and at the same time the radial position of the stack is changed (e. g. by changing the magnetic guide field) in such a way that the increased stack width just fills the radial aperture which was first needed for injection. The radial aperture taken by the fast inflector is about 5 cm, so that by

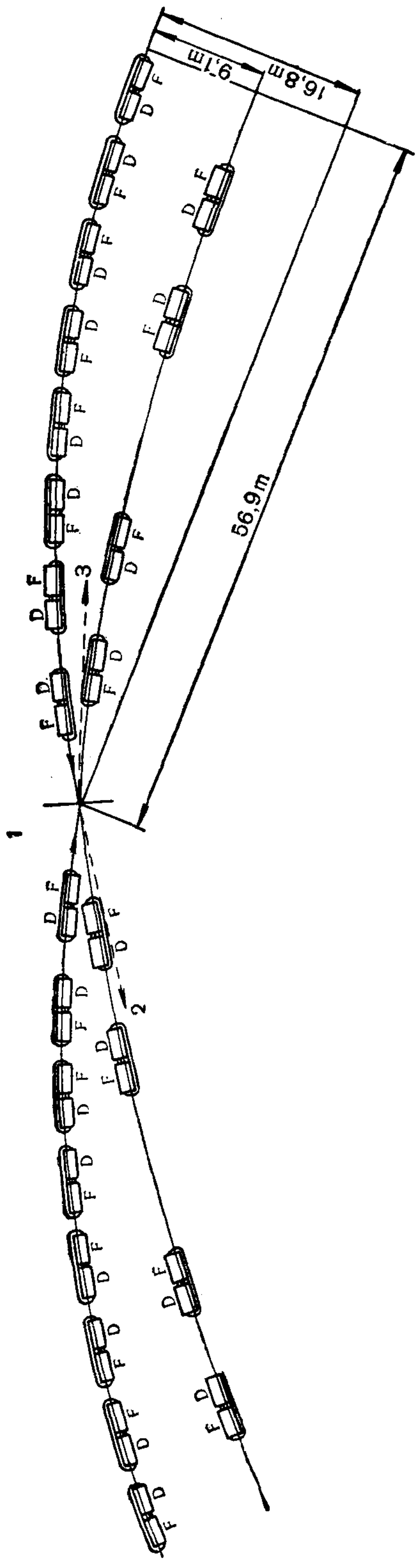

Fig. 2. Layout of the concentric storage ring magnets:
1 — interaction region; *2* — scattered proton 2; *3* — scattered proton 1.

this procedure practically no beam is lost. For some experiments it may be important to have the smallest possible vacuum chamber in the interaction region. In such a case one can inject with the quadrupoles for the Terwilliger scheme already excited. The maximum current is then approximately a factor 2 smaller but the ISR vacuum chamber in the interaction straight sections could be round thin walled pipes with a diameter of about 5 cm. The normal vacuum chamber size is $4 \times 15\,\mathrm{cm}^2$.

Fig. 2 shows the layout of the ISR magnet units. They are strong focusing with a pole profile and aperture very similar to that of the CERN PS. The free length of the long straight sections, in between the magnet coils, is about 12 m. In half of the interaction regions the beams go towards the outside of the ISR, in the other half they go towards the inside. The free sections downstream of the interaction region are the longest in the latter case so that these interaction regions are most suitable for small angle scattering experiments.

3. GENERAL CHARACTERISTICS OF COLLIDING BEAM INTERACTIONS

In order to design a pair of ISR which permit efficient utilisation one should have reasonable predictions of the angular ranges in which the secondary particles are produced. Although the center-of-mass is at rest (apart from a small velocity component due to the crossing angle of the beams) the angular distribution of the secondaries is far from isotropic, as is well known. Predictions of the angular distribution of elastically scattered protons in 25 GeV colliding beam reactions, based on extrapolations of measurements at the CERN PS and using the theory of the shrinking of the diffraction peak, have been made by Taylor [4]. In Table 1 we have reproduced his figures in a convenient form. The first column gives the scattering angle ϑ and the second column gives the number of elastically scattered protons $dN/d\omega$ per steradian per colliding beam event. Since $dN/d\omega$ changes so rapidly with ϑ the angular resolution of a scattering experiment should be better than 1 mrad. The third column therefore shows the total number of protons per colliding beam event that are elastically scattered into a solid angle $2\pi \sin \vartheta d\vartheta$ with $d\vartheta = 1$ mrad. The latter figure is a measure for the maximum obtainable counting rate in an experiment. Since the ISR magnets severely restrict the accessible solid angles the counting rate in an actual experiment will in general be an order of magnitude lower. The largest angle at which useful counting rates can be obtained is between 40 and 50 mrad.

Table 1

ϑ (mrad)	$\frac{dN}{d\omega}$ (per ster. per colliding beam event)	$\frac{dN}{d\omega} \cdot 2\pi \sin\vartheta \cdot 10^{-3}$ (per colliding beam event)
0	400	1.2×10^{-2}
5	375	1.7×10^{-2}
10	275	9×10^{-3}
15	90	2×10^{-3}
20	18	3×10^{-4}
25	2	6×10^{-5}
30	0.3	5×10^{-8}
40	2×10^{-4}	6×10^{-11}
50	2×10^{-7}	4×10^{-11}
60	1×10^{-8}	4×10^{-12}
70	1×10^{-9}	4×10^{-13}
80	1×10^{-10}	5×10^{-14}

Let us now consider the inelastic p-p collisions. Angular distributions in the cms for 29.5 GeV stationary target experiments have been given by Cool [5] and turn out to be very anisotropic. In fact the experimental information both from accelerators and cosmic rays is approximately consistent with the assumption that the average transverse momentum of secondaries depends neither on their longitudinal momentum nor on the energy of the primary particle. Cocconi et al. [6] have proposed the following distribution function for the transverse momentum of secondaries

$$g(p_\perp)\,dp_\perp = \frac{p_\perp}{p_0^2} \exp\left(-\frac{p_\perp}{p_0}\right) dp_\perp, \qquad (1)$$

where the average transverse momentum is $2p_0 \approx 0.45$ GeV/c. Using this formula we find that half of the secondaries have a production angle smaller than $0.38/p$, where p is the total momentum in GeV/c. The smallness of the transverse momentum seems to hold for all presently known particles. If new heavy particles would be produced in the ISR it is probable that their production will also occur at rather small angles.

For momenta of a few GeV/c the average production angles derived from eq. 1 are considerably larger than for elastic p-p scattering, but they still fall in a range where serious interference with the ISR magnets occurs and these must therefore be designed with this requirement in mind. It is probable that reactions with a large momentum transfer, and therefore large production angles, will be among the most interesting ones. However, no reliable predictions for the cross-section of such reactions exist and since particle detection at large angles is much easier than at small angles, we shall in the following mainly concentrate our attention on reactions at small angles.

4. BACKGROUND DUE TO RESIDUAL GAS

An accurate calculation of the background due to residual gas is practically impossible, but on the other hand a good estimate of this background is very important to evaluate the experimental possibilities of the ISR. For the calculation presented in this section we had to make several simplifying assumptions, but we expect it nevertheless to give the correct order of magnitude of the background.

We shall assume that the residual gas in the ISR vacuum chamber is N_2 at a pressure of 10^{-10} mm Hg. This pressure is within the limits of present ultra high vacuum technique [7], but little is known about the composition of the residual gas. With cryogenic pumping in the interaction region the pressure could be made even lower and the residual gas would probably be mainly H_2 and He. Therefore these assumptions may well be on the conservative side. The total cross-section of 25 GeV protons on nitrogen nuclei is about 380 mb. With a current of 20 A the number of beam-gas interactions is then 3.4×10^2 per cm of vacuum chamber per sec.

In the following we shall be especially concerned with elastic and nearly elastic *p-p* scattering. The two questions about background are then the following:

1. How many elastic beam-gas scatterings look like elastic beam-beam scatterings?
2. What is the total counting rate, irrespective of particle type or momentum in a counter placed close to the ISR vacuum chamber?

To answer 1) we assume that the ratio between elastic and total cross-section and the angular distribution of the elastically scattered protons from nitrogen nuclei is the same as from free target protons. Using the data of Taylor we have calculated the number of protons per beam-gas event per ster. that are elastically scattered at an angle ϑ. The result is shown in the second column of Table 2. The third column of this table gives the momentum difference ΔP between incident and scattered proton. Up to 40 mrad ΔP is smaller than the momentum spread of the circulating beam so that one cannot distinguish between elastic beam-beam and elastic beam-gas scattering by means of momentum analysis. As discussed in section 6 this difficulty can be overcome by detecting the two elastically scattered protons from the colliding beam events in coincidence.

Table 2

ϑ (mrad)	$\frac{dN}{d\omega}$ (per ster. per beam-gas event)	ΔP (GeV/c)
0	400	0
5	375	0.008
10	325	0.032
15	150	0.075
20	45	0.134
25	13	0.208
30	3	0.30
40	0.16	0.53
50	8×10^{-3}	0.83
60	2×10^{-3}	1.20
70	6×10^{-4}	1.63
80	2×10^{-4}	2.13

A counter telescope set at an angle ϑ sees a total length of beam d/ϑ, where d is the width of the beam, that we take as 1.5 cm. If ω is its angular acceptance the flux of protons which are elastically scattered from the gas nuclei is about $\frac{5\times10^2\,\omega}{\vartheta}\times\frac{dN}{d\omega}$.

To answer 2) we shall make a number of simplifying assumptions. The elastically scattered protons hit the vacuum chamber at such a small angle that their average path in it is close to 1 nuclear mean free path. We shall therefore assume that all beam-gas interactions are inelastic and concentrated in a line source with Q interactions per unit length per sec located in the centre of the vacuum chamber. The influence of the ISR magnetic field is neglected. Let us call $\left(\frac{dN}{d\omega}\right)_t$ the total number of secondaries independent of their momentum which are produced per ster. per beam-gas interaction at an angle ϑ. One can readily show, that the total flux in an annular counter of width w, concentric with the vacuum chamber is then

$$\phi = 2\pi w Q \int_0^{\pi/2} \left(\frac{dN}{d\omega}\right)_t \cos\vartheta \, d\vartheta \qquad (2)$$

independent of its radius. Reasonably complete angular distributions have only been measured for π^- (paper [5] and unpublished CERN results). Using these data and Cocconi's (1961 a) universal curves [6] we have integrated eq. 2 and find that the π^- flux in an annular counter of width $w = 1$ cm is $\phi_{\pi^-} = 5 \times 10^3$/s.

The total number of π^+ and π^0 is the same as that of the π^-. The π^0 decays into 2 γ's which have a good chance of being converted in the vacuum chamber wall. We shall therefore take $\phi_{\pi^+} = \phi_{\pi^-}$ and $\phi_{\pi^0} = 4\ \phi_{\pi^-}$. Inspection of the angular distribution of secondary protons shows that their average energy is much higher than that of the π^- but that their total number is roughly equal to that of the π^- at most angles. We therefore take $\phi_p = \phi_{\pi^-}$. Adding up we find $\phi = 3.5 \times 10^4$/sec. for $w = 1$ cm.

The ISR magnets should have rather little influence on the numbers calculated above. Their main effect is to create an extra flux of degraded nuclear particles, low energy electrons and γ's. From eq. 2 it is seen, that the contribution of a particle to the background flux in the vicinity of the ISR vacuum chamber is proportional to $\cos\vartheta$. The degraded particles are more isotropic and therefore they contribute less to the background flux than the first generation secondaries concidered above. Moreover shielding with some suitably placed lead bricks may eliminate a large fraction of the degraded particles. A reliable calculation is very difficult and we shall quite arbitrarily multiply the flux calculated above by a factor 2. The total flux in a 1 cm wide annular counter is then

$$\phi_{\mathrm{tot}} = 7 \times 10^4/\mathrm{sec} \qquad (3)$$

and we shall use this number in the following to estimate background fluxes.

5. MEASUREMENT OF THE TOTAL *p-p* CROSS-SECTION

The number of colliding beam events per second is

$$N_{bb} = \int_{-1/2h}^{1/2h} \frac{N_{t_1}(z)\, N_{t_2}(z)}{(2\pi R)^2} \, \frac{c\sigma}{\mathrm{tg}\,\frac{\alpha}{2}} \, dz \qquad (4)$$

where $N_{t1}(z)\,dz$ and $N_{t2}(z)\,dz$ are the total number of protons between z and $z + dz$ independent of their radial position in the two ISR, R — average radius of the ISR, h — beam height, α — crossing angle of the beams, c — velocity of light and σ — total *p-p* cross-section. We assume that the vacuum chamber is a 5 cm diameter thin walled pipe and that the circulating current is 10 A. A possible counter setup to measure N_{bb} is shown in Fig. 3. S_1, S_2, S_1' and S_2' are 80 cm diameter counters placed at 0.6 and 6 m from the interaction region. The vacuum chamber passes through holes in the counters. S_1 and S_1' count the secondaries produced at large angles, while the particles passing through the hole in S_1 and S_1' are counted by S_2 and S_2', unless their emission angle is smaller than 5 mrad. The outputs of S_1 and S_2 and of S_1' and S_2' are in parallel. A coincidence between $(S_1 + S_2)$ and $(S_1' + S_2')$ is considered as a colliding beam event.

Elastic scattering mainly occurs at very small angles and has nearly constant differential cross-section for $\vartheta < 5$ mrad. By making measurements with different holes in the counters and extrapolating down to $\vartheta = 0°$ it might be possible to separate the inelastic and elastic cross-sections with this counter arrangement. In this layout the main source of background are secondaries from beam-gas reactions, which pass through S_1 and S_1'. To eliminate these it is necessary to use directional Cherenkov counters, arranged in such a way that S_1 and S_2 count only particles travelling from left to right and S_1' and S_2' only particles travelling in the opposite direction.

Using the background calculation of the preceding section we find that the particle flux in $S_1 + S_2$ is 3×10^6/sec. However, the counting rate is much smaller, since practically all secondaries from beam-gas events are relativistic and will arrive at the same time in the counter, producing one large pulse. We shall therefore take the counting rate in $S_1 + S_2$ as equal to the total number of beam-gas events in 10 m of vacuum chamber. The average velocity of light in a plastic scintillator, due to its index of refraction and increase of the light path by reflections is about 1/3 of c. In view of the size of the counters we shall assume a time resolution $\tau = 10^{-8}$ s. The accidental coincidence counting rate $(S_1 + S_2) + (S_1' + S_2')$ is then

$$2\tau N(S_1 + S_2)\, N(S_1' + S_2') = 500/\mathrm{sec} \qquad (5)$$

which is about 1% of the colliding beam event rate at 10 A.

The absolute counting rates of about 10^5/sec are high but well within the possibilities of fast electronics, especially since the duty cycle is 100%. On the other hand a beam current of 1 A would be entirely sufficient for a total cross-section measurement. It is interesting to note, that the ratio of signal to accidental coincidences is independent of the number of stacked protons, since both are proportional to the square of the circulating beam current. The simplest and most accurate method to measure $N_{t_1}(z)$ and $N_{t_2}(z)$ is to insert a thick target from above or below into the beam and to measure the surviving circulating beam current as a function of target position. This is a destructive measurement that can only be made after the counting run has been completed, but since the whole experiment could be done in a few hours, during which beam blow up due to gas scattering or other undesirable effects can certainly be kept very small, this is not a serious restriction.

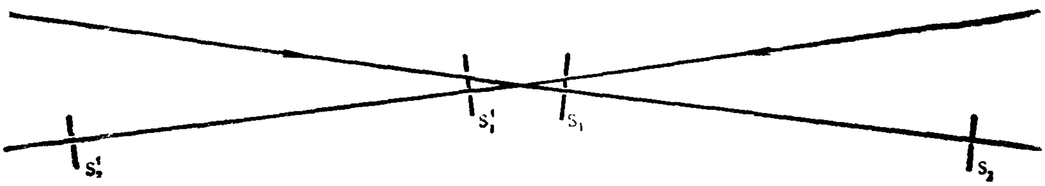

Fig. 3. Counters for p-p total cross section measurement.

6. ELASTIC p-p SCATTERING

As we have seen in sec. 3 an elastic p-p scattering experiment is limited to angles below 50 mrad by the rapid decrease of the cross-section. At these small angles the scattered protons pass so close to the ISR magnet units, that there is no place for separate momentum analyzing magnets [8]. The natural solution is therefore to extend the gap of the ISR magnets in the radial direction, so that they can serve at the same time as analyzing magnets for the scattered protons. A possible design for an extended strong focusing magnet is shown in Fig. 4. On the closed side of the gap the poles have been extended with the same gap height as the magnet aperture on the equilibrium orbit, namely 10 cm. It is difficult to make a similar extension on the open side of the gap, since this would disturb the magnetic field distribution in the ISR aperture. Trajectories of protons, that are elastically scattered in diametrically opposite directions are shown in Fig. 2, and we see that scattered proton 1 can be momentum analyzed by extending radially outward the first F half magnet sector downstream of the interaction region. Scattered proton 2 can be momentum analyzed by extending radially inward the first D half magnet sector downstream of the interaction region. With the FOFDOD structure shown in Fig. 2 this leads to magnet units with a rather complicated shape while the product of gap height × magnetic field in the extension is limited by the fact that it should be equal to that on the ISR equilibrium orbit.

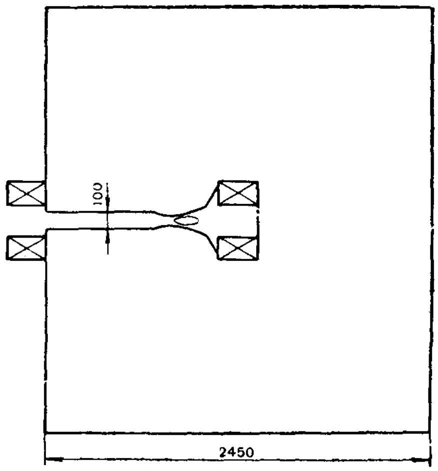

Fig. 4. Extended strong focusing magnet for small angle scattering experiments.

A completely different approach is shown in Fig. 5. The two strong focusing magnets downstream of the interaction region have been replaced by a homogeneous field magnet B_1 and a pair of quadrupoles Q_1 and Q_2. Orbit studies have shown that this leads to

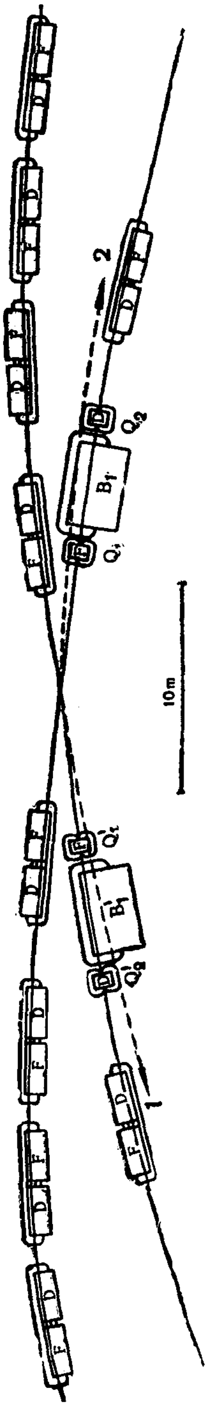

Fig. 5. Intersecting storage rings with special magnet sections: *1* — scattered proton 2; *2* — scattered proton 1.

an increase in betatron oscillation amplitude and stack width of only about 10%. Since the ISR operate with dc the adjustment of the magnetic field in the various magnets should present no special difficulties. The quadrupoles should be made with an open median plane, as shown in Fig. 6, since they should obstruct the scattered particle as little as possible. The momentum resolution of the magnet B_1 is a factor 2 better than that of the extended half strong focusing unit, while the gap height could easily be made 20 cm or more, with a corresponding increase of solid angle subtended at the interaction region. We shall assume therefore that the magnet layout of Fig. 5 is used for the elastic scattering experiment.

Trajectories of protons that are elastically scattered in the median plane are shown in Fig. 7. We shall now describe in some detail, how the differential cross-section for elastic *p-p* scattering at 30 mrad could be measured. This angle is representative for the range from 15 to 40 mrad. Afterwards we shall make a few comments on scattering measurements below 15 mrad. We shall assume that the beam width in the interaction region is reduced to 1.5 cm by using the Terwilliger scheme and that the circulating current is 20 A. It is not sufficient to observe only one of the scattered protons and to extrapolate back its trajectory to see if it came from the interaction region. With a beam width of 1.5 cm there are 1.5/0.030 = 50 cm of beam that can give elastic beam-gas scattering with the orbit of the scattered proton (or its prolongation) passing through the interaction region. Comparison of Tables 1 and 2 shows that at $\vartheta = 30$ mrad, $\frac{dN}{d\omega}$ for elastic beam-gas

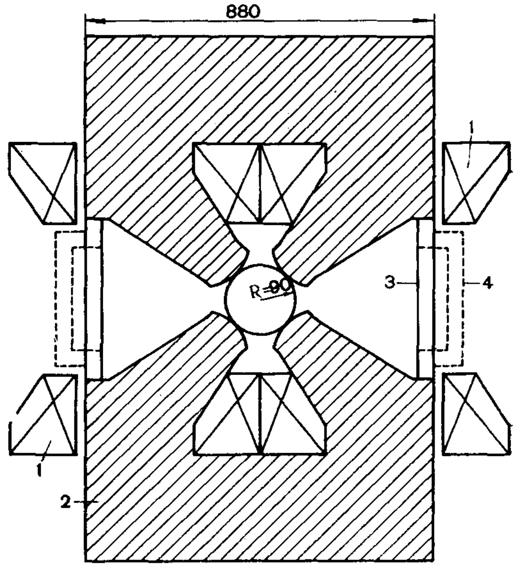

Fig. 6. Quadrupole with open median plan: *1* — coil; *2* — yoke; *3* — support; *4* — alternative support.

scattering is 10 times larger than $\frac{dN}{d\omega}$ for elastic beam-beam scattering so that the ratio signal to background would be about one to one. Therefore it is necessary to detect the two elastically scattered protons in coincidence. Momentum analysis is also necessary in order to discriminate against inelastic *p-p* scattering or the production of two π's in opposite directions.

The layout of the detectors is also shown in Fig. 7. Proton 1 passes through spark chambers SC_1 and SC_2 which measure its production angle and through SC_3 and SC_4 which measure its deflection in B_1. S_2 and S_4 are triggering counters. The proton scattered in the opposite direction is detected by a similar set of spark chambers SC'_1 to SC'_4 and counters S'_2 and S'_4. The experiment counts all protons which are scattered in the angular interval

29 mrad $< \vartheta <$ 31 mrad. The vertical angular acceptance is ± 7 mrad if the gap height of B_1 and B_1' is 20 cm. The total solid angle is then 2.8×10^{-5} sr and from Table 1 we find a rate of 1.3 good events/sec.

The maximum angles of the proton orbits in the circulating beam, due to horizontal betatron oscillations are about ± 0.3 mrad. If the spark chambers which detect the scattered proton are 4 m apart, and the accuracy of spark location is ± 0.5 mm, the angular resolution within 2%. The criterium on the angles is probably the more stringent of the two.

If the Terwilliger scheme is not used, the stack width is 6 cm and apart from the smearing out due to the 1.5 cm width of the injected beam, the proton energy increases with increasing radius. By extrapolating back the trajectories of the two scattered protons one can find the point of interaction and determine its radial position in each of the two ISR. From this one can derive the energy of each

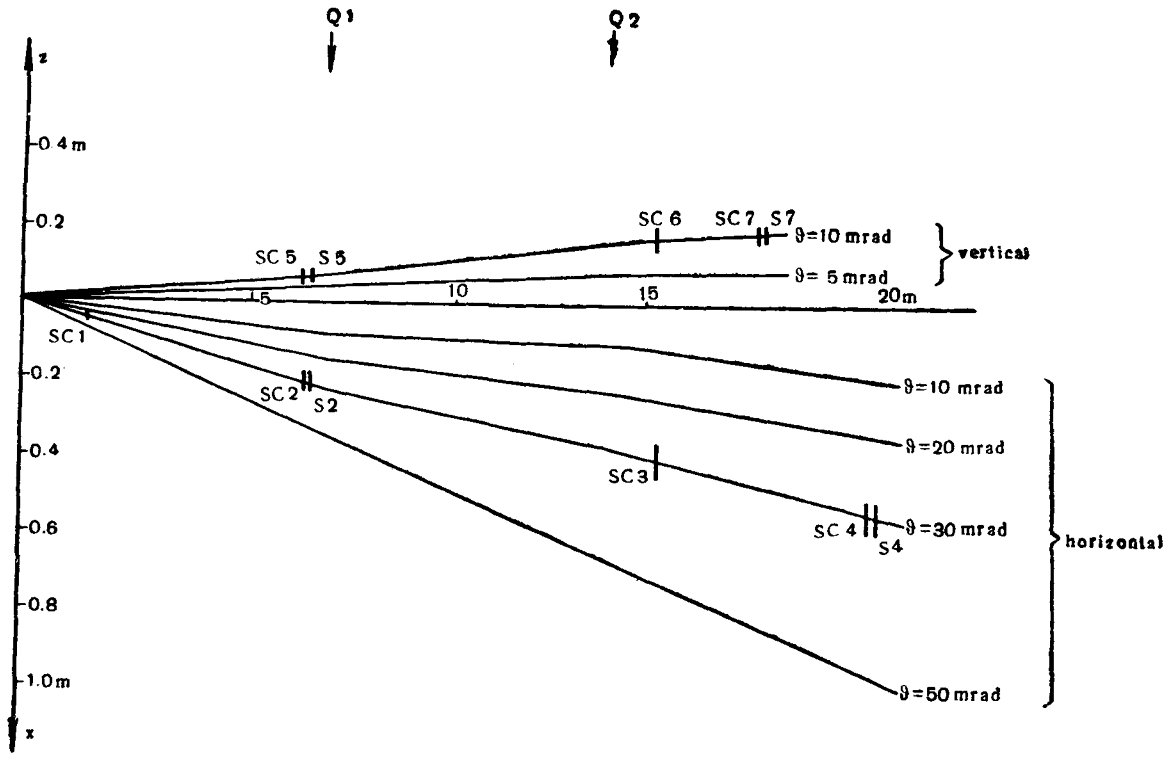

Fig. 7. Trajectories of elastically scattered protons and location of spark chambers.

is ± 0.25 mrad. The deflection in B_1 is 67 mrad and therefore the momentum resolution is about $\pm 0.75\%$, whereas the momentum spread in the circulating beam was $\pm 1.25\%$. We see therefore that the limits on the experimental resolution due to the properties of the circulating beam and those of the detector are comparable. As selection criteria to distinguish between good and bad events one can use that the two scattered protons should go in diametrically opposite directions within 1 mrad and that their momentum should be equal to the average momentum of the circulating beam of the two primary protons with an accuracy of $\pm$ 0.3%. With a wider beam the counters and spark chambers must be larger and will collect more background. The best method of operation will therefore vary from one experiment to another. In this paper we shall always assume that the Terwilliger scheme is used.

The purpose of the spark chambers is to obtain a good angular and momentum resolution in a geometry over which the experimenter has little control. The stray fields of Q_1 and Q_1' are rather inhomogeneous and it may also be uneconomical to extend the poles of B_1

so far that the field through which the proton passes, is homogeneous. Accurate measurements of the magnetic field distribution will be necessary for the data analysis. We assume that the sensitive time of the spark chambers is 0.4 μs. Using the background data estimated in sec. 4 we then find that the probability that a spurious track occurs in any of the four spark chambers SC_1 to SC_4 when they are triggered on a good event, is about 10%. With a resolution time $\tau = 5 \times 10^{-9}$ s of the coincidence circuits we estimate that the accidental triggering rate is about 2×10^{-3}/sec.

Below 15 mrad it becomes difficult to find place to make exit windows for the scattered protons in the ISR vacuum chamber. Since the vertical aperture is only $\pm$ 2 cm it is better to use scattering in the vertical plane for very small angles. This is possible if the gap height of the special magnets B_1 and B_1' is large enough. The trajectory of a proton that is scattered through a vertical angle of 10 mrad is shown in Fig. 7, where we have also indicated a possible location of the spark chambers. For scattering angles down to 2 mrad the protons pass throught SC_6 and SC_7, but it is difficult to determine which solid angle is subtended at the interaction region.

7. INELASTIC *p-p* SCATTERING

Experiments by Cocconi et al. [9] at the CERN PS have shown that the energy spectrum of protons scattered at small angles has 2 bumps somewhat below the elastic peak. This is interpreted as the formation of two excited isobars via the reaction

$$p + p \to p + W. \qquad (6)$$

The masses of the excited isobars are $W_1 = 1.51$ GeV and $W_2 = 1.69$ GeV. We shall now discuss how reaction (6), if it should occur, could be measured with colliding beams. The momentum loss of the proton in this case is

$$\Delta P = \left(\frac{W^2}{M^2} - 1\right)\frac{Mc}{4\gamma}, \qquad (7)$$

where M—proton rest mass and γMc^2—total energy of the colliding protons, which we take as 25 GeV. Substitution gives

$$\left.\begin{aligned} \Delta P_1 &= 14 \text{ MeV/c for } W_1; \\ \Delta P_2 &= 20 \text{ MeV/c for } W_2. \end{aligned}\right\} \qquad (8)$$

These values are much too small to observe reaction (6) by momentum analysis of the scattered proton. The latter must therefore be detected in coincidence with at least one of the decay products of the W. For simplicity we shall neglect the three body decays of the W. If W_1 and W_2 are respectively the 2nd and 3rd πN resonances with isotopic spin $T = 1/2$, then we expect that they will decay according to

$$\left.\begin{aligned} W &\to p + \pi^0 \quad \text{(a)}; \\ W &\to n + \pi^+ \quad \text{(b)}. \end{aligned}\right\} \qquad (9)$$

with a ratio of (a)/(b) = 1/2. The total energies of the decay products are for W_1

$$\left.\begin{aligned} E_\pi &= 7.40 \cos\varphi + 7.77 \text{ GeV}; \\ E_p &= 7.40 \cos\varphi + 17.25 \text{ GeV} \end{aligned}\right\} \qquad (10)$$

and for W_2

$$\left.\begin{aligned} E_\pi &= 8.45 \cos\varphi + 8.73 \text{ GeV}; \\ E_p &= 8.45 \cos\varphi + 16.29 \text{ GeV}, \end{aligned}\right\} \qquad (11)$$

where φ is the decay angle in the rest system of the W with respect to its direction of flight. We restrict ourselves to detecting the charged decay products. It appears best to detect the p or π^+ near $\varphi = 0$ since at small angles E_p and E_π vary slowly with φ and the transformation of solid angles from the W rest system to the laboratory system is most favourable. For $\varphi = 0$ we find $E_\pi = 15.17$ GeV or $E_\pi = 17.18$ GeV and $E_p = 24.65$ GeV or $E_p = 24.74$ GeV. The relative energy spread in the circulating beam produces an approximately equal relative spread in E_π and E_p and therefore measurements on the decay proton appear marginal. Fortunately the values of E_π have a comfortable difference and are far below the elastic proton peak. The laboratory angle ψ with respect to the flight direction of the W at which the π^+ is produced is approximately

$$\left.\begin{aligned} \psi &\approx \varphi/33 \text{ for } W_1; \\ \psi &\approx \varphi/29 \text{ for } W_2. \end{aligned}\right\} \qquad (12)$$

Let us now consider how the elastic proton scattering experiment at 30 mrad could be modified to detect the scattered proton and the decay π^+ in coincidence. The branch SC_1 to SC_4, which detects the proton remains unchanged while the branch SC_1 to SC_4' now accepts all π^+ produced within $\pm$ 7 mrad horizontal angular acceptance and the dispersion in B_4'. Trajectories of π^+ mesons and the spark chamber locations are shown in Fig. 8.

By measuring the direction of the scattered proton one knows the direction of the W within 1 mrad. From ψ we can calculate φ and $\cos\varphi$ to correct the measured π^+ momentum for the decay angle φ. With $\Delta\psi = 1$ mrad and for a maximum production angle $\psi = 14$ mrad we find an uncertainty in the correction $\Delta E_\pi = 0.12$ GeV. The momentum spread in the circulating beam and the inaccuracy of momentum analysis give a maximum $\Delta E_\pi = 0.50$ GeV. Therefore the peaks belonging to the two excited isobars should be well separated in the π^+ spectrum.

Assuming isotropic decay of the W in its rest frame we find that SC_4' to SC_4' have a probability of 1.2×10^{-2} for detecting the π^+. The measurements of Cocconi et al. show that the probability for formation of an excited isobar is roughly the same as for elastic scattering. Since we assumed that 2/3 of the W's decay into $n + \pi^+$ the total counting rate of good events is 8×10^{-3} times the counting rate for elastic p-p scattering and amounts to 10^{-2}/sec.

The discussion of the background follows the same lines as for elastic p-p scattering. With a spark chamber sensitive time of 0.4 μs the probability of finding a spurious track in any of the spark chambers SC_4' to SC_4' when they are triggered, is about 30%. We estimate that with a suitable choice of triggering counters the accidental triggering rate can be made of the order of 2×10^{-3}/sec. A more detailed discussion of these figures has been given in another report [10].

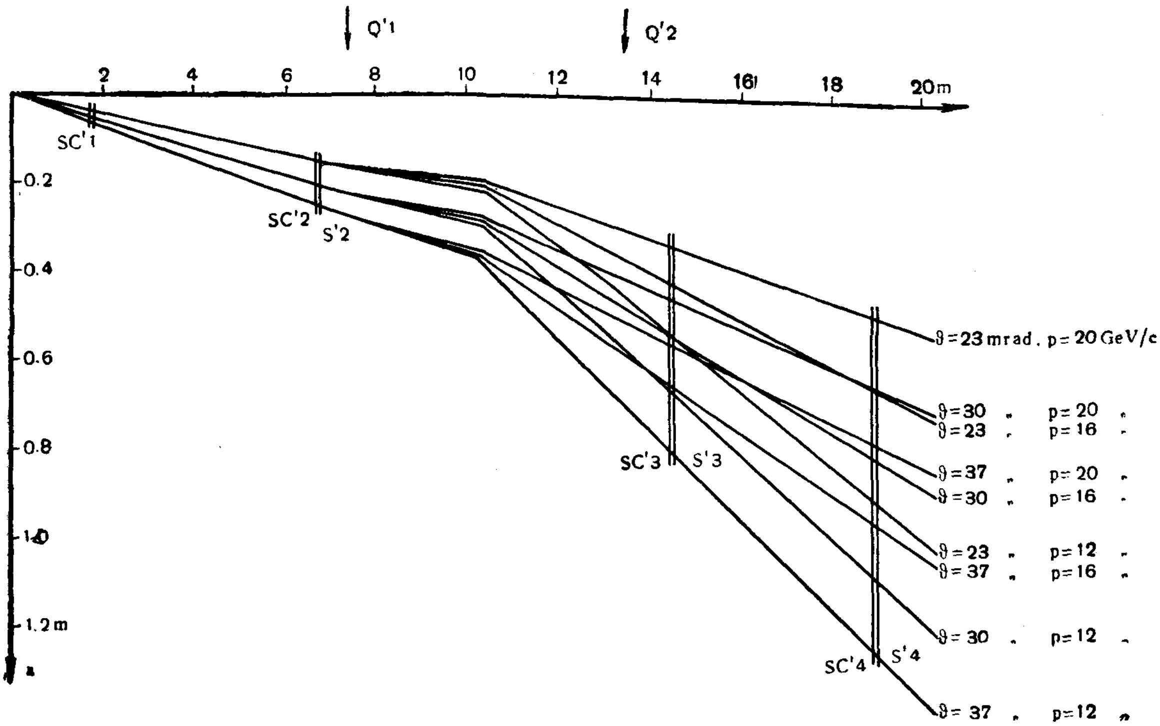

Fig. 8. Horizontal trajectories of π^+ with different momenta, produced at various angles ϑ.

8. 4π DETECTOR

The previous chapters were devoted to small angle scattering experiments which involve only a few particles. The average number of secondaries produced in an inelastic collision will be about 10. Measurements of secondary particle production spectra at different angles yield a limited amount of information since these data can only be treated statistically. For the search of correlations (resonances) between different particles originating from the same interaction one must perform the experiment in such a way that all secondaries from the same interaction can be observed simultaneously. This is then analogous to the present bubble chamber technique. There exist practically no preidictions about the type of inelastic interactions that could be studied with colliding beams and therefore we shall restrict ourselves to a few remarks about the practical aspects of a 4π detector.

The use of a bubble chamber for this purpose meets with various difficulties. At the present state of the art a bubble chamber can not be triggered, it has a sensitive time of a few tenths to one msec so that it collects a large number of background tracks and finally a bubble chamber with a length of a few meters is a bulky and expensive device. It appears therefore that also as a 4π detector the spark chamber is the most sûitable instrument. It is cheaper, can easily be made in large sizes and has a sensitive time which is reasonably matched to the particle fluxes in colliding beam experiments. Its triggered operation is of particular value. The total number of colliding beam interactions is 1.6×10^5/sec but it would be sufficient to record only a few complete events per second. This makes it possible to select particular events by means of suitable triggering counters. Let us assume, that a 4π spark chamber would collect background from about 10 m of vacuum chamber in both ISR. With an 0.4 μs sensitive time the probability of recording a beam-gas event when the spark chamber is triggered on a colliding beam interaction is 0.28. The probability of recording 2 colliding beam events is 0.06.

For momentum analysis the 4π spark chamber must have a magnetic field. The most obvious magnet design is the one discussed by O'Neill [11] and Jones [12] and which is shown again in Fig. 9. With a proper choice of magnet dimensions the return flux which also crosses the circulating beam can be made to cancel the effect of the main flux. The gap height of the main pole should be about 1 m. In principle it would be sufficient to give the return poles the same gap height as the ISR bending magnets. Since most secondaries, especially those with higher momenta, are produced at rather small angles to the circulating beam, the return flux is probably more useful than the main flux for their momentum analysis. It looks advisable, therefore, to give the return poles the same gap height as the main pole. By also placing coils around the return poles their stray field and its influence on the ISR magnet units is kept small. The magnet shown in Fig. 9 has massive poles since we assume that sparks can be located with acoustic pickups or alternately that stereo photographs can be made from the side by means of suitably disposed mirrors. Due to its large gap height the main pole has an important stray flux and its steel will already be completely saturated (3 Wb/m²) for 1.6 Wb/m² in the interaction region. Higher fields would require excessive amounts of power. The magnet of Fig. 9 would consist of 350 t steel, 80 t copper and consume 5 MW.

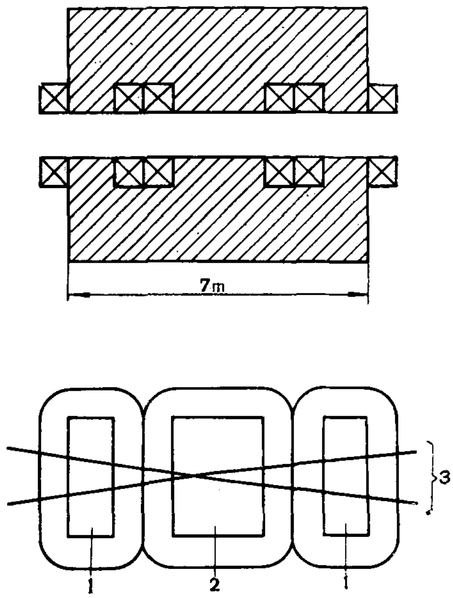

Fig. 9. Magnet for 4π spark chamber: *1* — returne pole; *2* — main pole; *3* — circulating beams.

Like the circulating beam the orbits of secondaries will have a kink so that they emerge from the return pole in the same direction as at production but laterally displaced by a distance *d*. If *d* is large enough the orbit can never fit inside the vacuum chamber and must always show up somewhere in the spark chamber. Table 3 shows for different momenta

Table 3

Momentum (GeV/c)	Δd for positive particles (cm)	Δd for negative particles (cm)
25	0	6.2
20	0.3	7.0
15	2.1	8.3
10	4.7	10.9
5	12.5	18.7

the value of Δd, the lateral displacement with respect to the circulating beam.

No negative particles and no positive particles below 10 GeV/c can remain undetected in the spark chamber. By placing additional spark chambers behind the first ISR magnet unit downstream of the interaction region a good fraction of the positive secondaries above 10 GeV/c which do not leave the ISR vacuum chamber in the interaction straight section, can also be detected.

To allow a good momentum measurement a particle must have a reasonably long visible path in the magnetic field. For high energy secondaries we shall assume that the momentum is «well measurable» if their orbit is at 3 cm or more from the vacuum chamber center at 1.5 m from the interaction region. In that case their full path in the return field is visible. The fraction F of particles which does not satisfy this condition, has been calculated with eq. 1 and is shown in Table 4. The small values of F for negative particles result from the large angle at which they must be produced to be unmeasurable.

Table 4

Momentum (GeV/c)	F for positive particles	F for negative particles
25	0.82	0.05
20	0.49	0.05
15	0.26	0.04
10	0.12	0.02
5	0.01	0

The values of F are not too good for positive particles but very low for negatives. However, even $F = 0$ does not solve all problems, since neutrals will escape detection anyhow.

It would be of great value in strange particles could be identified either because they decay outside the vacuum chamber or because one can extrapolate back the orbits of their decay products. The mean free path for decay λ of various unstable particles at a momentum of 10 GeV/c is given in Table 5. Using eq. 1 one can readily show that the probability that a particle will decay outside the vacuum chamber, considered as a straight pipe of radius r is

$$P_{\text{out}} = \frac{M^2}{p_0^2 c^2} \int_0^\infty y \exp\left(-\frac{My}{p_0 c} - \frac{r}{c\tau y}\right) dy \quad (13)$$

independent of its longitudinal momentum. In this equation M—particle rest mass, τ—particle life time. Taking $p_0 = 0.225$ GeV and $r = 3$ cm we have given in the last column of Table 5 the value of P_{out}.

Table 5

Particle	λ (cm) at 10 GeV/c	P_{out}
ϑ	61	0.26
Λ	70	0.31
Σ^-	44	0.17
Σ^+	21	0.16
Ξ^-	41	0.06

Of the particles listed in Table 5 only the ϑ(75%) and Λ (58%) can decay into two charged particles. The others always have at least one neutral decay product so that their decay can only be recognised from a sudden change in direction of the track. This is only possible if the particles decay reasonably far outside the vacuum chamber.

Assuming a $\pm$ 0.5 mm accuracy in spark location we estimate that for 50% of the Λ's and for 90% of the ϑ's decaying inside the vacuum chamber the point of decay can be found by extrapolating back the trajectories of the secondaries with an accuracy of $0.1\ \lambda$. This is roughly independent of momentum since λ is proportional to p but the angle between the decay products is proportional to $1/p$. We conclude therefore, that the detection efficiency for ϑ and Λ is quite good but that for the other particles the identification of their decay will in general be difficult.

9. SHIELDING AND BUILDINGS

From eq. 3 we see that if collisions with the residual gas at a pressure of 10^{-10} mm Hg were the only source of background, the radiation level in the vicinity of the ISR vacuum chamber would exceed the maximum permissible dose by at least two orders of magnitude. This means that even under these ideal conditions the spark chambers are never accessible in the presence of a stacked beam. If access to the spark chambers is required, the only possibility is to dump the stacked beams and it takes about one hour of CERN PS operation to fill both ISR again. The electronic triggering circuits must be close to the spark chambers to avoid delays in the cables but on the other hand they must be shielded from the ISR to make them continuously accessible for repairs.

When the vacuum is temporarily less good than the value assumed above, the background increases correspondingly. During the filling of the ISR the background due to protons which are lost from the stack, is much larger. The stacked beams themselves are potentially dangerous sources of radiation, since they contain some 10^{15} protons and it is always possible that the beams would be lost near an interaction region due to faulty operation of an experimental magnet, vacuum troubles etc. Although in principle one can design a fast kicker magnet which dumps the beam in a well shielded place in case of accidents, such a system could in our opinion never be absolutely safe. Finally the ISR may quite often be used as beam stretchers for the CERN PS. All these arguments taken together lead to the conclusion that the shielding thickness of the ISR must be comparable to that of the CERN PS.

A reliable estimate of the dimensions required for the experimental areas around the interaction regions is very difficult. The experiments discussed in the preceding sections would indicate that the width of these halls need not be too large, since both the small angle scattering experiments and the 4π detector as we envisage it, have only moderate lateral dimensions. It is not clear, however, to what extent these experiments are representative for the way in which the ISR will be used. Adequate space in the vicinity of the interaction region must also be foreseen to assemble the large experimental magnets and spark chambers described in this report.

We have assumed therefore a width of 25 m for the colliding beam areas and this should be enough for most experiments. The side walls of these halls must be made in such a way that parts of it can easily be removed to make a passage for a beam. In this way future extensions are always possible. The beam height above the floor in the interaction region should be at least 4 m. The length of the experimental areas has been chosen as 50 or 70 m. The height under the crane hook should be about 10 m. We shall now indicate three different solutions for the shielding and building design:

1. The colliding beam halls could be constructed with light walls and roof and the ISR shielded with movable blocks and roof beams. In principle this arrangement is very flexible but there are some practical problems connected with it. To keep the roof shielding beams reasonably short, one must place the concrete walls rather close to the ISR. A change of the experimental setup will therefore usually necessitate the shifting of substantial quantities of concrete. This is time consuming and may also affect the alignment of the ISR.

2. Another solution is suggested by the fact that the site adjacent to the CERN PS, which is available for the ISR is not very flat. The ground level is lowest in the region marked «external target hall» and is about 10 m higher at the diametrically opposite side of the ISR. Due to the bad mechanical properties of the surface ground layer the ISR floor level near the external target hall has to be several meters below the ground surface, and therefore the ISR building is completely underground at the opposite side, so that shielding on the sides is automatically provided. By making the roof of the colliding beam area sufficiently strong so that it can support 3.2 m of earth (the same as on top of the CERN PS tunnel) one obtains a shielded tunnel with a free width of 25 m, which would be quite convenient for the experiments discussed in this report.

3. An intermediate solution is to make a hall with a strong roof, covered with 3.2 m of earth, but with light side walls, apart from a number of pillars to support the roof. Shielding on the sides is then provided by a wall of shielding blocks along the outside of the building. This method also leaves the possibility open for extensions. We intend to place different types of building around different interaction regions, both in order to adopt them to different types of experiments and to find a solution that minimizes the total cost of excavation, foundations, movable shielding and buildings. The work on the experimental area layout and buildings will form an important part of our study program for intersecting storage rings.

REFERENCES

1. Hereward H. G., Johnsen K., Schoch A. and Zilverschoon C. J. In Proceedings of the International Conference on High Energy Accelerators (Brookhaven, 1961), p. 265.
2. O'Neill G. K. In Proceedings of the International Conference on High Energy Accelerators (CERN, 1959), p. 125.

3. Terwilliger K. M. *Ibid.*, p. 53.
4. Taylor A. E. Comparison of Elastic $p-p$ Scattering from Colliding Beams and Stationary Targets. CERN Report AR/Int. SG/62-11, Contribution 14 (1962).
5. Cool R. L. In Proceedings of the International Conference on High Energy Accelerators (Brookhaven, 1961), p. 15.
6. Cocconi G., Koester L. J. and Perkins D. M. Calculation of Particle Fluxes from Proton Synchrotrons of Energy 10—1000 GeV, Lawrence Radiation Lab. UCID—1444 (1961).
7. Fischer E. See this edition, p. 347.
8. Jones L. W. and de Raad B. Nucl. Instr. and Meth., **20**, 477 (1963).
9. Cocconi G. et al. Phys. Rev. Lett., **7**, 450 (1961).
10. de Raad B. Design of Some Experiments with Proton Storage Rings, CERN AR/Int. SG/62-12 (1962).
11. O'Neill G. K. In Proceedings of the International Conference on High Energy Accelerators (CERN, 1959), p. 23.
12. Jones L. W. *Ibid.*, p. 15.